Hybrid statistics-simulations based method for atom-counting from ADF STEM images

Hybrid statistics-simulations based method for atom-counting from ADF STEM images

Annelies De wael[a], Annick De Backer[a], Lewys Jones[b], Peter D. Nellist[b], Sandra Van Aert[a]

[a]*Electron Microscopy for Materials Science (EMAT), University of Antwerp, Groenenborgerlaan 171, 2020 Antwerp, Belgium*
[b]*Department of Materials, University of Oxford, Parks Road, OX1 3PH Oxford, UK*

Abstract

A hybrid statistics-simulations based method for atom-counting from annular dark field scanning transmission electron microscopy (ADF STEM) images of monotype crystalline nanostructures is presented. Different atom-counting methods already exist for model-like systems. However, the increasing relevance of radiation damage in the study of nanostructures demands a method that allows atom-counting from low dose images with a low signal-to-noise ratio. Therefore, the hybrid method directly includes prior knowledge from image simulations into the existing statistics-based method for atom-counting, and accounts in this manner for possible discrepancies between actual and simulated experimental conditions. It is shown by means of simulations and experiments that this hybrid method outperforms the statistics-based method, especially for low electron doses and small nanoparticles. The analysis of a simulated low dose image of a small nanoparticle suggests that this method allows for far more reliable quantitative analysis of beam-sensitive materials.

Keywords: annular dark field scanning transmission electron microscopy (ADF STEM), statistical parameter estimation theory, atom-counting, beam-sensitive nanomaterials

1. Introduction

The physical properties of nanostructures are controlled by their composition, their chemical bonding and the positions of their atoms. At the nanoscale, the properties of materials are strongly size-dependent [1, 2, 3]. This size dependence opens up many possibilities for the production of nanomaterials with unique properties, but also demands an accurate and precise quantification of their size. An excellent technique to study nanostructures is atomic resolution scanning transmission electron microscopy (STEM) [4, 5]. The intensities in annular dark field scanning transmission electron microscopy (ADF STEM) monotonically depend on the atomic number Z and on the thickness of the material [5, 6, 7, 8], which makes this imaging mode particularly suitable for performing a quantitative analysis of nanostructures [9, 10, 11], such as atom-counting [12, 13]. By counting the number of atoms in each atomic column from two-dimensional (2D) ADF STEM images recorded under a few different viewing directions, a three-dimensional (3D) reconstruction of the structure can be obtained [13, 14], allowing for the quantification of the shape and size of the nanoparticle. Furthermore, atom-counting results can be combined with ab-initio calculations or Monte Carlo simulations to study the dynamical behaviour of nanoparticles [15, 16, 17, 18].

At present, two methods exist for counting the number of atoms from ADF STEM images, based either on image simulations [12, 16] or on statistical parameter estimation theory [13, 19, 20]. In the present paper, these methods will be referred to as the image simulations-based method and the statistics-based method. In order to count the number of atoms, the total scattered intensity corresponding to each atomic column in the nanoparticle is first quantified by the so-called scattering cross section. These scattering cross sections are calculated by integrating the image intensity in circles [21] or Voronoi cells [16, 22] around the position of the atomic column, or by estimating the volumes under Gaussian peaks which are fitted to the atomic columns [10, 19, 20, 23].

The image simulations-based method is very intuitive, as it directly compares experimental scattering cross sections to simulated scattering cross sections [12, 16]. However, using this method, systematic errors in the image simulations are difficult to detect, since such a direct thickness assignment is always possible. In other words, the accuracy of the obtained atom-counts depends on the unknown accuracy of the experimental parameters used as an input for the image simulations, such

as for example the detector angles or the mistilt of a sample away from a perfect zone-axis [24]. Furthermore, this method does not provide a measure for the precision of the atom-counts. It is worth noting that over the last few years, techniques for the characterisation of these experimental parameters have strongly improved [24, 25, 26, 27, 28, 29].

Alternatively, in the statistics-based method, unknown structure parameters are estimated by fitting an incoherent parametric imaging model to the experimental images using a criterion of goodness of fit [10, 19, 20, 23, 30, 31]. Based on these estimated structure parameters, estimates for the scattering cross sections can be obtained. These estimates are then used as an input for a second parameter estimation step. The set of scattering cross sections can be decomposed into components, each generated by a set of columns with the same number of atoms. Due to the unavoidable presence of noise, these components cannot be discriminated visually. To retrieve these components, the set of scattering cross sections is regarded as a statistical draw from an underlying, unknown probability distribution. The parameters of this probability distribution are estimated by maximising the likelihood of the probability distribution [13, 19, 20, 32]. Based on the estimated probability distribution, atom-counts are assigned to the atomic columns. The described statistics-based method is very reliable and results in atom-counts with single atom sensitivity [20], provided the inherent limitations of the method are not exceeded [19, 33]. The atom-counts obtained by the statistics-based method for very small nanoparticles are often unreliable due to the limited number of columns present in the image [19, 33]. Furthermore, the performance of the statistics-based method is very sensitive to a low signal-to-noise ratio [19, 33]. The increasing relevance of radiation damage, not only in biological studies, but also in the study of nanostructures [34], demands a method that allows for a reliable quantitative analysis of low dose images with a low signal-to-noise ratio. The hybrid statistics-simulations based method is proposed to overcome the limitations of the statistics-based method, and thus progress towards the quantitative analysis of small, beam-sensitive materials. This hybrid method will be realised by incorporating prior knowledge about the material, obtained by carefully performing image simulations, into the statistics-based method.

The outline of the present paper is as follows. The methodology of the proposed hybrid method is discussed in section 2, and then applied to a HAADF STEM image of a gold nanorod in section 3. Next, in section 4, the possibilities and limitations of this improved method are examined, and a comparison with the statistics-based method is performed. Then, in section 5, the hybrid method is applied to a challenging experimental example, a very small platinum-iridium nanoparticle, imaged using a relatively low electron dose. Up to now, atoms could not be counted reliably from such an image. This case study will therefore be used to evaluate the amount of improvement of the hybrid method as compared to the statistics-based method. Finally, an image of the same nanoparticle, simulated such that the electron dose is more than ten times lower, is analysed, showing the possibilities for quantitative analysis of challenging beam-sensitive nanomaterials using low electron doses.

2. Methodology

First, the total scattered intensity belonging to each atomic column is quantified by estimating the scattering cross sections for each atomic column. To this end, an incoherent parametric imaging model consisting of 2D Gaussian peaks is fitted to the experimental image using a least-squares criterion [10, 19, 20, 23, 30, 31], as defined in Appendix A. Due to the unavoidable presence of noise, the set of scattering cross sections is regarded as a statistical draw from an underlying, unknown probability distribution, which can be described by a superposition of 1D Gaussian components, called a Gaussian mixture model [13, 19, 20]:

$$f_{\text{mix}}\left(\hat{V}_n;\boldsymbol{\Psi}_G^{\text{stat}}\right)=\sum_{g=1}^{G}\pi_g\phi_g\left(\hat{V}_n;\mu_g,\sigma\right), \qquad (1)$$

with

$$\phi_g\left(\hat{V}_n;\mu_g,\sigma\right)=\frac{1}{\sqrt{2\pi\sigma^2}}\exp\left(-\frac{(\hat{V}_n-\mu_g)^2}{2\sigma^2}\right), \qquad (2)$$

with σ the width of the components, μ_g the location of the g^{th} component, π_g the mixing proportion of the g^{th} component, $\hat{V}_n$ the scattering cross section of the n^{th} column, and $\boldsymbol{\Psi}_G^{\text{stat}}$ the parameter vector

$$\boldsymbol{\Psi}_G^{\text{stat}}=(\pi_1,...,\pi_{G-1},\mu_1,...,\mu_G,\sigma)^T, \qquad (3)$$

containing the $2G$ parameters to be estimated using the statistics-based method. Note that π_G is not estimated, since the mixing proportions sum up to unity. Unlike the statistics-based method, the hybrid method puts constraints on the locations μ_g of the Gaussian mixture model. These constraints are based on prior knowledge from image simulations. Therefore, image simulations

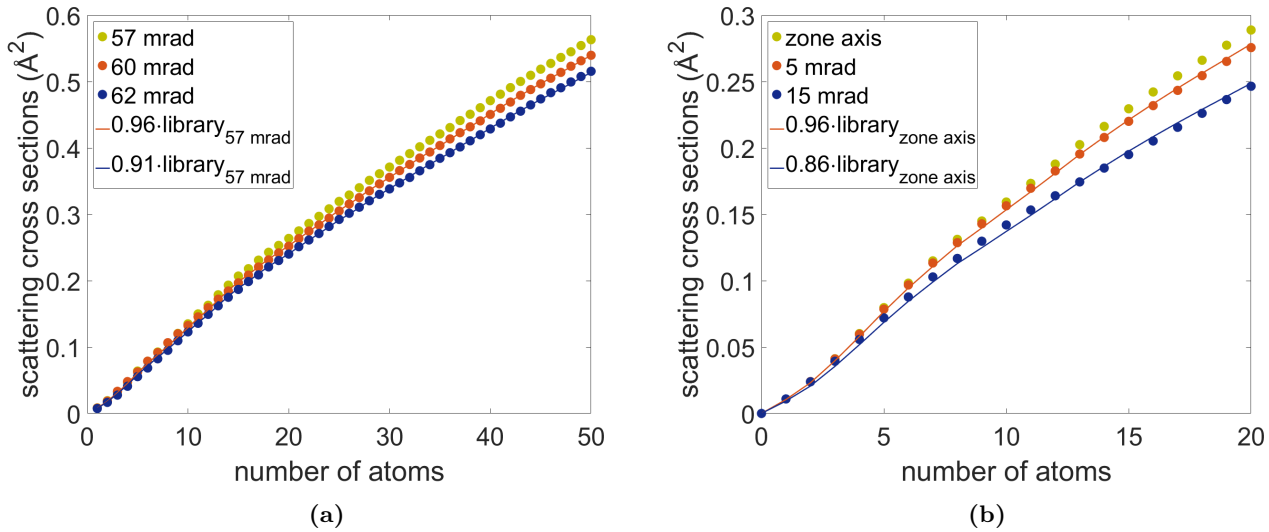

Figure 1: The effect of slightly different experimental parameters on the scattering cross sections evaluated as a function of the number of atoms per column can be approximated by a linear scaling. (a) Simulated scattering cross sections for Au in [100] zone axis obtained with different detector inner angles. (b) Simulated scattering cross sections for different values of the sample tilt around the [001] axis. Solid lines show scaled libraries. Colour online.

need to be performed for different thicknesses. The experimental parameters that describe the imaging conditions used to record the ADF STEM image are used as an input for the image simulations and should therefore be measured as accurately as possible. The scattering cross sections calculated from these simulated images of atomic columns with different thicknesses compose the so-called library. The prior knowledge is included into the hybrid method by assuming that the locations of the components correspond to scaled library values:

$$\mu_g = a\mathcal{M}_g, \tag{4}$$

where a is an unknown scaling parameter and $\mathcal{M}_g$ represents the library value of the g^{th} component, corresponding to columns with g atoms. This implies that the number of parameters to be estimated reduces from $2G$ to $G+1$:

$$\mathbf{\Psi}_G^{\text{hybrid}} = (\pi_1, ..., \pi_{G-1}, a, \sigma)^T. \tag{5}$$

The probability distribution for the hybrid method is therefore expressed as follows:

$$f_{\text{mix}}\left(\hat{V}_n; \mathbf{\Psi}_G^{\text{hybrid}}\right) = \sum_{g=1}^{G} \pi_g \phi_g\left(\hat{V}_n; a, \sigma\right), \tag{6}$$

with

$$\phi_g\left(\hat{V}_n; a, \sigma\right) = \frac{1}{\sqrt{2\pi\sigma^2}} \exp\left(-\frac{(\hat{V}_n - a\mathcal{M}_g)^2}{2\sigma^2}\right). \tag{7}$$

By estimating the scaling parameter a to determine the locations of the components of the probability distribution, we take into account possible unknown discrepancies between actual and simulated experimental conditions. Figure 1 shows simulated scattering cross sections evaluated as a function of the number of atoms per column for different values of the detector inner angle or sample tilt. The solid lines in both figures indicate that linearly scaled libraries are a good approximation for the scattering cross sections simulated using different parameters. In figure 1a, simulated scattering cross sections for Au in [100] zone axis obtained with different detector inner angles 57 mrad, 60 mrad and 62 mrad are shown. The scattering cross sections simulated using an inner angle of 60 or 62 mrad can be approximated by linearly scaling the scattering cross sections corresponding to 57 mrad, acting as the library in this example. These detector inner angles correspond to reasonable measurement errors in the detector inner angle of upto ±5 mrad [24]. In figure 1b, simulated scattering cross sections are shown for a sample tilt around the [001] axis, upto 15 mrad, which can experimentally still yield an atomic resolution image [24]. Also in this case, the scaled library for the sample in zone axis is an acceptable approximation for the scattering cross sections corresponding to different sample tilt values.

The updates of the parameters of the probability dis-

tribution used in the hybrid method are derived by maximising the likelihood function:

$$L(\mathbf{\Psi}_G^{\text{hybrid}}) = \prod_{n=1}^{N} f_{\text{mix}}\left(\hat{V}_n; \mathbf{\Psi}_G^{\text{hybrid}}\right), \tag{8}$$

or equivalently, by minimising the negative log likelihood function, with respect to the parameters π_g, a and σ. Updates for these parameters are calculated using the iterative EM-algorithm [32] and are given by the following expressions:

$$\pi_g^{(k+1)} = \frac{1}{N}\sum_{n=1}^{N} \tau_g\left(\hat{V}_n; \mathbf{\Psi}_G^{\text{hybrid},(k)}\right), \tag{9}$$

$$a^{(k+1)} = \frac{\sum_{n=1}^{N}\sum_{g=1}^{G} \tau_g\left(\hat{V}_n; \mathbf{\Psi}_G^{\text{hybrid},(k)}\right)\hat{V}_n\mathcal{M}_g}{\sum_{n'=1}^{N}\sum_{g'=1}^{G} \tau_{g'}\left(\hat{V}_{n'}; \mathbf{\Psi}_G^{\text{hybrid},(k)}\right)\mathcal{M}_{g'}^2}, \tag{10}$$

$$\sigma^{(k+1)} = \sqrt{\frac{1}{N}\sum_{g=1}^{G}\sum_{n=1}^{N} \tau_g\left(\hat{V}_n; \mathbf{\Psi}_G^{\text{hybrid},(k)}\right)\left(\hat{V}_n - a^{(k)}\mathcal{M}_g\right)^2}, \tag{11}$$

with

$$\tau_g\left(\hat{V}_n; \mathbf{\Psi}_G^{\text{hybrid},(k)}\right) = \frac{\pi_g^{(k)}\phi_g(\hat{V}_n; a^{(k)}, \sigma^{(k)})}{\sum_{g'=1}^{G}\pi_{g'}^{(k)}\phi_{g'}(\hat{V}_n; a^{(k)}, \sigma^{(k)})}, \tag{12}$$

the posterior probability that the estimated scattering cross section of the n^{th} column $\hat{V}_n$ belongs to the g^{th} component. The index (k) indicates the iteration step. Reliable starting values of the mixing proportions π_g and the width of the components σ are given by the following expressions [19]:

$$\pi_g^{(0)} = \frac{1}{G}, \tag{13}$$

and

$$\sigma^{(0)} = \frac{\max(\hat{\mathbf{V}}) - \min(\hat{\mathbf{V}})}{2G}, \tag{14}$$

where $\hat{\mathbf{V}}$ represents the set of scattering cross sections. The starting values of the scaling parameter are more critical because of the presence of many local minima in the negative log likelihood as a function of the scaling parameter. Therefore, multiple starting values for the scaling parameter need to be used, ranging between a minimum and maximum expected scaling value, in order to ensure convergence to the correct model. For each of these starting values, the algorithm is iterated until convergence is reached. The estimates $\hat{\mathbf{\Psi}}_G^{\text{hybrid}}$ of the parameters in the Gaussian mixture model are then given by the set of estimated parameters corresponding to the model with the maximum likelihood.

A direct consequence of the prior knowledge included into the hybrid method by equation (4) is that the g^{th} component in the Gaussian mixture model is now always supposed to correspond to atomic columns with g atoms. Therefore, the number of components G will be called the "library length" from here on. Missing components are attributed a mixing proportion $\pi_g = 0$ by the hybrid method, and can therefore be easily recognised, whereas they are simply not estimated by the statistics-based method. This is an advantage, since in a real nanostructure it is quite feasible that no single atoms are present around the edge. The first non-zero component could therefore easily be at two or three atoms.

The above described algorithm provides atom-counts for a given library length G. Unfortunately this library length G is not known beforehand. In principle, a large enough library length can be used to obtain the same correct model, since mixing proportions of components that exceed the maximum thickness can be estimated zero. However, in practice, a smaller scaling parameter a in combination with non-zero proportions often results in a better fit of the Gaussian mixture model to the underlying scattering cross sections. The resulting model has a higher likelihood, but is not the correct model. A selection criterion therefore needs to be used to determine the physically meaningful library length, required to estimate the correct probability distribution. Such a criterion includes a likelihood term, as well as a penalty term. Many different information criteria exist, accounting for the complexity of the estimated model in a different manner [32]. The Integrated Classification Likelihood (ICL) criterion was shown to have the best performance for atom-counting [19]:

$$ICL(G) = -2\log L(\hat{\mathbf{\Psi}}_G^{\text{hybrid}}) + 2EN(\hat{\tau}) + d\log N, \tag{15}$$

with a negative log likelihood term $-2\log L(\hat{\mathbf{\Psi}}_G^{\text{hybrid}})$, and a penalty term $2EN(\hat{\tau}) + d\log N$ depending on the sample size N, on the number of parameters $d = G + 1$ to be estimated, and on the entropy, expressed by

$$EN(\hat{\tau}) = -\sum_{g=1}^{G}\sum_{n=1}^{N} \tau_g\left(\hat{V}_n; \hat{\mathbf{\Psi}}_G^{\text{hybrid}}\right)\log\tau_g\left(\hat{V}_n; \hat{\mathbf{\Psi}}_G^{\text{hybrid}}\right). \tag{16}$$

A high library length is penalised, while a higher likelihood is favoured, as to obtain a physically meaningful

trade-off between the goodness of fit and the complexity of the model. The methodology introduced in this section will now be applied to an experimental gold nanorod in the next section.

3. Counting the number of atoms in a gold nanorod

In this section, an experimental HAADF STEM image of a gold (Au) nanorod will be analysed in order to illustrate the methodology of the hybrid method for atom-counting. The number of atoms in this Au nanorod could already be counted reliably using the statistics-based atom-counting method [20], as an agreement between independent image simulations and the estimated locations was then found within the expected 5%-10% error range [20, 22, 35]. Therefore, this well-conditioned experimental example can be used to validate the results obtained with the hybrid method. The image was recorded along the [100] zone axis at the QuAntEM, a double corrected FEI Titan^3 working at 300 kV, and is shown in figure 2a.

The scattering cross sections calculated from the refined model of the experimental image are shown in figure 2b. In an ideal case, we would observe separated components, corresponding to the different thicknesses. However, due to the unavoidable presence of noise, these components are broadened and they therefore overlap each other. This broadening is described by the probability distribution given by equation (6)-(7). Such a probability distribution is then estimated for each library length ranging between 1 and 100. The values of the ICL criterion, given by equation (15), for each of these library lengths are evaluated in figure 2c. The top axis indicates the estimated scaling parameter corresponding to the models at different library lengths. In this example, the minimum of interest occurs at a library length equal to 51, corresponding to a scaling parameter of $a = 0.99$, reflecting the high accuracy of the measured experimental parameters. The estimated probability distribution at this library length is shown as a full black curve in figure 2b. The individual components are shown in colour, corresponding to the number of atoms per column. In figure 2d, each atomic column was assigned the number of atoms corresponding to the highest probability based on the estimated probability distribution from figure 2b.

The interpretation of the ICL criterion obtained by the hybrid method slightly differs from the interpretation of the ICL criterion as obtained by the statistics-based method. We are still looking for a local minimum, but additional information is provided by the value of the scaling parameter and can be used to determine the correct local minimum. Usually, multiple local minima, corresponding to different values of the scaling parameter, are present in the ICL criterion. If the experiment was conducted carefully, discrepancies between actual and simulated experimental conditions are expected to be small, i.e. within the expected 5%-10% error range [20, 22, 35]. This would imply a scaling value approximately equal to 1. However, it is inadvisable to discard other local minima based only on their unexpected scaling values. A local minimum at a scaling value which differs strongly from 1 can be selected as the minimum of interest when one can explain the nature of these large discrepancies, e.g. by means of additional image simulations using different values for sample tilt or inner detector angle. If this is not the case, the local minimum corresponding to a scaling value close to 1 is selected as the minimum of interest.

Note that inclined grey lines with slope $\log N$ are added to the plot of the ICL criterion. In the ICL criterion in figure 2c, we see linear features where the values increase parallel to the grey lines, i.e. with the same slope of $\log N$. These features indicate that the estimated probability distribution for these library lengths is essentially the same. In fact, the mixing proportions of components corresponding to a library length exceeding the first library length of the feature are estimated equal to zero. As a consequence, the entropy term and the likelihood term for these library lengths remain the same, leaving $d \log N$ as the only changing term in the expression for the ICL criterion given by equation (15). Such linear features indicate a very good mathematical fit to the data, and can be used for interpretation of the ICL minimum. However, such features may not always be present due to for example large amounts of noise. If such features appear and coincide with a scaling value close to 1, we can choose the first library length of the feature as the minimum of interest.

Figure 2e displays the difference between the atom-counts obtained by the hybrid method and the statistics-based method for each atomic column. On average the number of atoms per column differs by only 1.02 atoms between both methods. This confirms the reliability of the results obtained with the hybrid method. In the next section, the performance of the hybrid method will be examined in detail and compared to the statistics-based method.

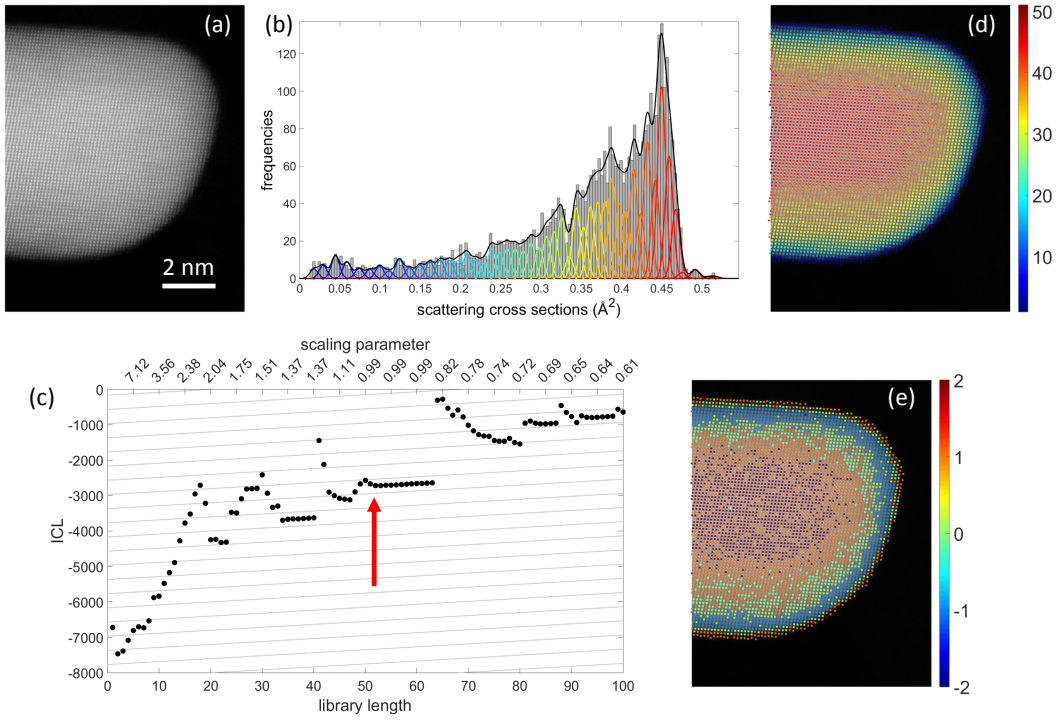

Figure 2: (a) HAADF STEM image of a gold nanorod [20]. (b) Set of scattering cross sections. The solid black curve shows the estimated Gaussian mixture model, whereas the coloured curves indicate the individual components. (c) ICL criterion, with two axes, indicating library length and estimated value of the scaling parameter a. (d) Atom-counts for the gold nanorod. (e) Difference in atom-counts between the hybrid method and the statistics-based method. Colour online.

4. Possibilities and limitations

4.1. Precision & accuracy of the estimated parameters

In the present section, we evaluate the accuracy and precision of the estimated parameters. Ultimately, in order to perform a reliable quantitative analysis, the parameters of the probability distribution of the scattering cross sections expressed by equation (6)-(7) need to be estimated as accurately and precisely as possible. A statistical estimator of a parameter is accurate when the expectation value of the estimator equals the actual value of the corresponding parameter. For such an unbiased estimator, a lower bound on the variance exists, which expresses the highest attainable precision. This lower bound on the variance is given by the so-called Cramér-Rao lower bound [36, 37], defined in Appendix B.

In order to assess the accuracy and precision of the estimated parameters by the hybrid method, 100 noise realisations were created by performing random draws from a Gaussian mixture model with 5 components and parameters π_g, a and σ for which the input values are given in table 1. For each noise realisation, the mixing proportions π_g for the different components are multinomially distributed with equal probabilities. Furthermore, an equally spaced library is used. The relative width of the components, defined as the ratio between the width of the columns σ and the average difference between the locations of successive components δ, equals $\sigma/\delta = 0.25$. The average number of observations per component equals $N/G = 20$. The parameters were estimated by the hybrid method using starting values for the mixing proportions π_g and the width of the components σ given by equations (13) and (14), and multiple starting values for the scaling parameter as discussed in section 2. The values of the estimated parameters, obtained at the correct library length, are summarised in table 1 and confirm that the parameter estimates are accurate, as the input value of each parameter is enclosed by the 95% confidence interval on the sample mean. Table 2 summarises the sample variances of the parameter estimates for the same sets of scat-

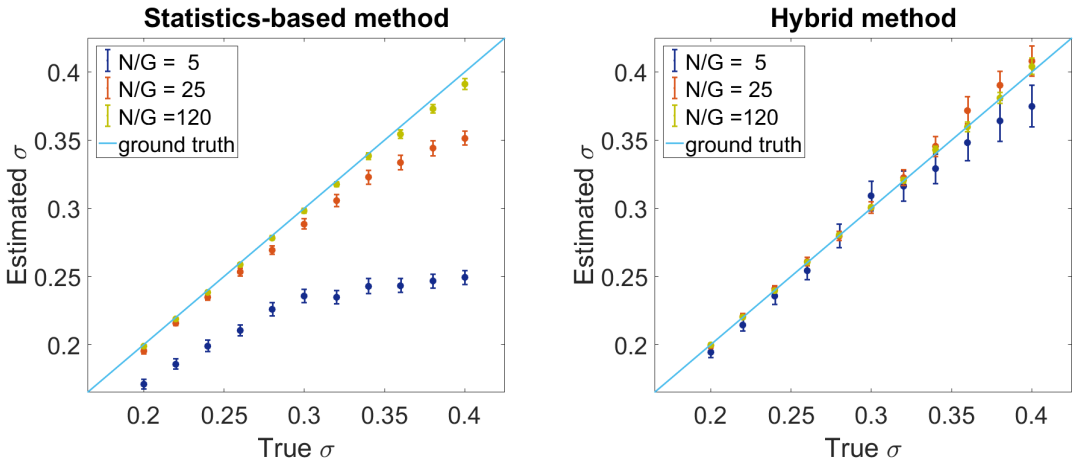

(a) (b)

Figure 3: Accuracy of the estimated width of the components σ. The estimated width of the components is evaluated as a function of the true value of σ used in the Gaussian mixture models for (a) the statistics-based method and (b) the hybrid method. Colour online.

tering cross sections used to validate the accuracy, together with a 95% confidence interval and the Cramér-Rao lower bound for each parameter. We conclude that the Cramér-Rao lower bound is indeed attained, as the 95% confidence intervals on the sample variances include the Cramér-Rao lower bound for each parameter. Thus, parameter estimates obtained by the hybrid method are obtained with the highest possible precision.

Parameter	Input value	Sample mean	95% confidence interval
π_1	0.2	0.2005	[0.1922; 0.2088]
π_2	0.2	0.1979	[0.1901; 0.2057]
π_3	0.2	0.1987	[0.1901; 0.2073]
π_4	0.2	0.1990	[0.1913; 0.2066]
π_5	0.2	0.2039	[0.1951; 0.2128]
a	1	0.9990	[0.9970; 1.0011]
σ	0.25	0.2468	[0.2427; 0.2508]

Table 1: Accuracy of the parameter estimates that determine the Gaussian mixture model estimated by the hybrid method. The sample means are computed from parameter estimates obtained from 100 noise realisations of the Gaussian mixture model and compared with the input values of the model parameters.

An important drawback of the statistics-based method is the underestimation of the value of the width of the components σ in case of a small average number of columns per component N/G [19]. In order to assess the accuracy of the estimated width of the components, noise realisations were again created by performing random draws from Gaussian mixture models with 10 components, in the same manner as described before. Different combinations of N/G and σ/δ were used, and 100 noise realisations were performed for each of these combinations. In figure 3 the estimated width of the components is evaluated as a function of the true width of the components, for different values of the average number of columns per component N/G. Estimated widths are shown for both the statistics-based method and the hybrid method, with 95% confidence intervals. We conclude from figure 3 that the hybrid method provides more accurate estimates for the width of the components as compared to

Parameter	CRLB	Sample variance	95% confidence interval
π_1	0.0017	0.0018	[0.0013; 0.0023]
π_2	0.0018	0.0016	[0.0017; 0.0020]
π_3	0.0018	0.0019	[0.0013; 0.0025]
π_4	0.0018	0.0015	[0.0015; 0.0019]
π_5	0.0017	0.0021	[0.0016; 0.0026]
a	0.000098	0.00011	[0.000089; 0.00014]
σ	0.00044	0.00062	[0.00034; 0.00055]

Table 2: Precision of the parameter estimates that determine the Gaussian mixture model estimated by the hybrid method. The sample variances are computed from parameter estimates obtained from 100 noise realisations of the Gaussian mixture model and compared with the Cramér-Rao lower bound for the model parameters.

the statistics-based method, which severely underestimates the width of the components at low values of N/G. The parameter estimates for the width σ obtained by the hybrid method are thus more reliable, resulting in more reliable atom-counts, as compared to the statistics-based method. Furthermore, this implies that the hybrid method allows for a more accurate estimate of the relative width of the components σ/δ, which determines the overlap between Gaussian components. Therefore, the precision of the atom-counts themselves can be more accurately predicted, as this is inherently determined by the amount of overlap between the components.

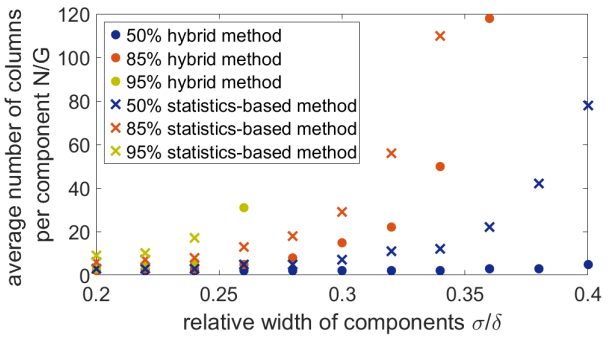

Figure 4: The average number of columns per component needed to obtain 50%, 85% or 95% correctly counted atomic columns by the hybrid method or the statistics-based method, for a certain relative width of the components. Colour online.

4.2. Atom-counting performance

The atom-counting performance can be quantified by the percentage of correctly counted atomic columns. Therefore, we will calculate this percentage obtained by the hybrid method for different combinations of the average number of columns per component N/G and the relative width of the components σ/δ, as well as for the statistics-based method. The relative width of the components σ/δ is large when the signal-to-noise ratio is low, as is for example the case for low dose images. The average number of columns per component N/G can be related to the size of the particle. A small particle corresponds to a small value of N/G. The values of σ/δ and N/G determine how difficult it is to count the number of atoms. They can therefore be referred to as the conditions for atom-counting. The largest improvement in the percentage of correctly counted atomic columns attained by the hybrid method is expected at difficult conditions for atom-counting, corresponding to noisy images of small nanoparticles.

Noise realisations were created by performing random draws from Gaussian mixture models with 10 components, as described in section 4.1. The values of σ and N are varied. For each combination, 100 such noise realisations were performed. The percentages of correctly counted atomic columns, after evaluation of the ICL criterion, are displayed in figure 4. The ICL criterion was evaluated between library lengths 8 and 12. The interpretation of the ICL criterion introduced in section 3 was applied in order to select the minimum of interest. The average number of columns per component N/G required to correctly count 50%, 85% and 95% of the atomic columns is evaluated as a function of the relative width of the components σ/δ. The percentage of correctly counted atomic columns increases with increasing average number of columns per component N/G and decreasing relative width of the components σ/δ. However, the required N/G to reach a given percentage with the hybrid method is lower than the N/G needed to reach the same percentage using the statistics-based method for constant σ/δ. In other words, the hybrid method does indeed outperform the statistics-based method, especially for small nanostructures. Note that the percentage of correctly counted atomic columns is determined by the selection of the library length after an evaluation of the ICL criterion on the one hand, and by the overlap between the Gaussian components, limiting the precision, on the other hand. We conclude from the results in figure 4 that the most significant improvement is achieved at high values of σ/δ. These results therefore suggest the possibility of reliably counting the number of atoms in samples where counting was previously impossible, specifically in images of small, beam-sensitive particles recorded using a lower electron dose. In the next section, a platinum-iridium nanoparticle recorded using a relatively low electron dose will be analysed using the hybrid method.

5. Counting the number of atoms in a platinum-iridium nanoparticle

In the present section, the hybrid method is used to count the number of atoms in a challenging experimental, relatively low dose image of a small Pt/Ir particle, shown in figure 5a and previously already analysed in [33]. The particle was supported on a three-dimensional carbon black support and was received in powder form dusted onto a carbon coated copper grid. The image was taken at the QuAntEM, a double corrected FEI Titan^3 working at 300 kV. The difference in atomic number between Ir (Z=77) and Pt (Z=78) is only one, causing a difference of less than 3% in the scattering cross sections up to 15 atoms in a projected atomic column. Therefore, Pt and Ir can be analysed together for the purpose of counting

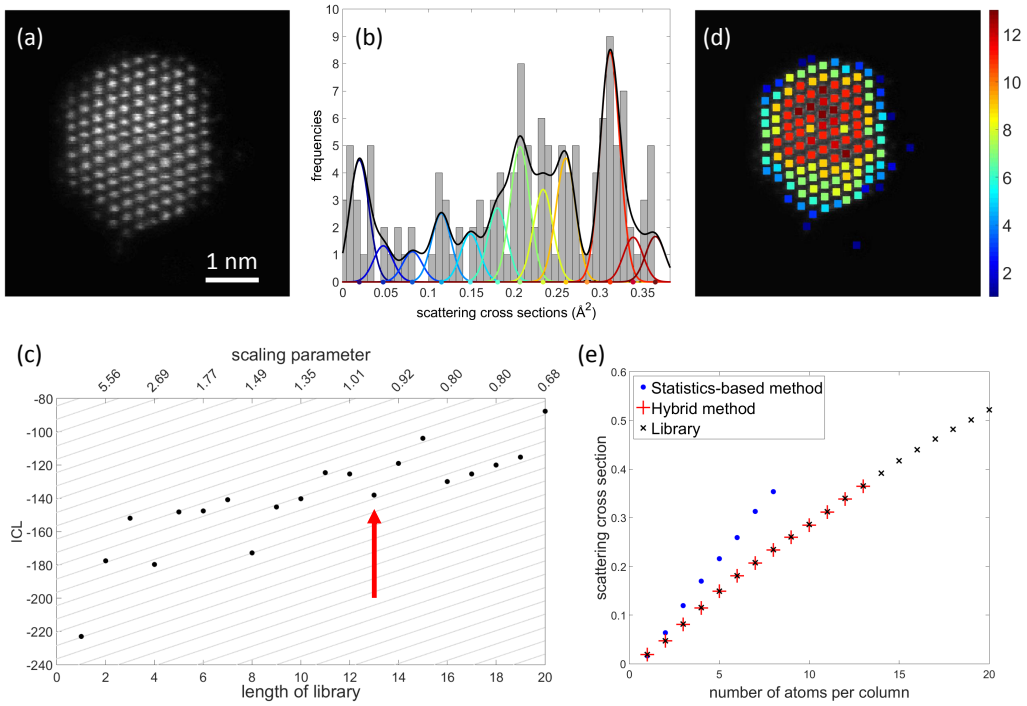

Figure 5: (a) **Experimental** ADF STEM image of a platinum-iridium nanoparticle recorded using a dose of $6.5 \cdot 10^4$ $e^-/\mathring{A}^2$ [33]. (b) Set of scattering cross sections. The solid black curve shows the estimated Gaussian mixture model, whereas the coloured curves indicate the individual components. (c) ICL criterion, with two axes, indicating library length and estimated value of the scaling parameter a. (d) Atom-counts for the platinum-iridium nanoparticle. (e) Scattering cross sections evaluated as a function of the number of atoms per column. Colour online.

the number of atoms per column. Simulated cross sections were calculated from image simulations assuming Pt only. Using the statistics-based method, a significant mismatch between the estimated locations and the simulated scattering cross sections was found [33]. It was shown that the statistics-based method underestimates the model order due to the insufficient electron dose.

Figure 5 summarises the analysis of this relatively low dose image of the Pt/Ir particle using the hybrid method. The set of estimated scattering cross sections is shown in figure 5b. By assessing the ICL criterion as a function of the library length and the scaling parameter, the minimum of interest is chosen at the significant local minimum which occurs at library length 13, as indicated in figure 5c. The estimated scaling parameter at this library length is close to the expected value of 1. The resulting estimated probability distribution of the scattering cross sections is shown in figure 5b by a black curve. The individual components that compose the distribution are displayed in different colours. In figure 5d, each atomic column was assigned the number of atoms corresponding to the highest probability based on the estimated probability distribution. It is clear from figure 5e that a good agreement with the image simulations is now achieved. This intensity/thickness graph evaluates the estimated locations by the statistics-based method, the scaled library values, corresponding to the estimated locations by the hybrid method, and the library values, i.e. the simulated scattering cross-sections, as a function of the number of atoms per column. A mismatch between estimated cross sections and simulated cross sections is no longer found by the hybrid method, since the scaling parameter is estimated almost equal to 1. The hybrid method therefore enables us to overcome the limitations of the statistics-based method. Note that the local minimum in the ICL criterion at library length 16 should also be considered. The corresponding scaling parameter of 0.8 can however not be explained. High dose experiments on the same day confirm that the detector inner angle was accurately determined and visual interpretation of

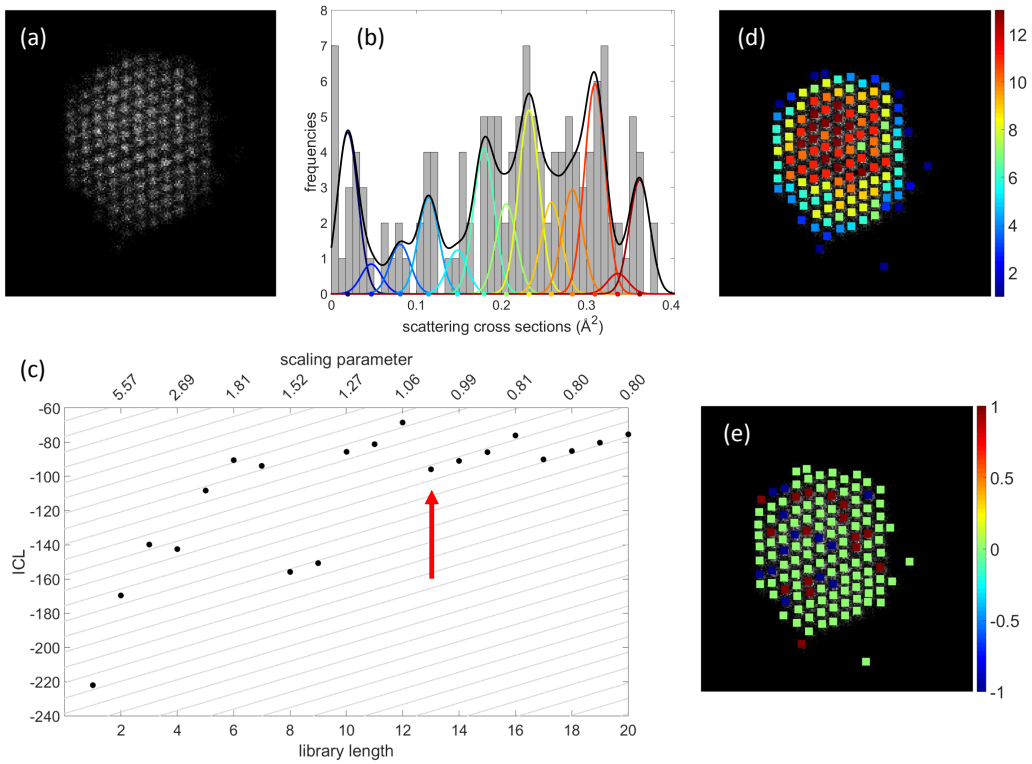

Figure 6: (a) **Hypothetical** ADF STEM image corresponding to a low electron dose of 10^3 $e^-/\mathring{A}^2$, based on the platinum-iridium nanoparticle from figure 5. (b) Set of scattering cross sections. The solid black curve shows the estimated Gaussian mixture model, whereas the coloured curves indicate the individual components. (c) ICL criterion, with two axes, indicating library length and estimated value of the scaling parameter a. (d) Atom-counts for the simulated low dose image of a nanoparticle. (e) Difference in atom-counts between original image and the simulated lower dose image. Colour online.

the image excludes a large sample tilt. Therefore, we have sufficient arguments to accept the local minimum at the scaling value closest to 1.

Thus far, we have shown that the hybrid method enables us to reliably count the number of atoms per column in an experimental image from which reliable atom-counting was previously impossible due to an insufficient electron dose. In order to investigate the possibilities for very low electron doses, a hypothetical low dose image of a small nanoparticle is now treated with the hybrid method. This analysis is summarised in figure 6. The simulated image is obtained by performing a Poisson distributed random draw from the model fitted to the Pt/Ir nanoparticles, corresponding to an electron dose of only 10^3 $e^-/\mathring{A}^2$. The resulting image is shown in figure 6a. The estimated scattering cross sections obtained from this image are displayed in figure 6b. Based on the ICL criterion from figure 6c, the minimum of interest is chosen at a library length of 13, as was also the case for the original image of the Pt/Ir nanoparticle. The corresponding scaling parameter is estimated equal to $a = 0.99$. The estimated probability distribution at this library length is shown in figure 6b. The lowering of the electron dose resulted in a broadening of the components estimated in the Gaussian mixture model from $\sigma/\delta = 0.3960 \pm 0.0049$ to $\sigma/\delta = 0.4243 \pm 0.0056$, resulting unavoidably in a more limited precision. However, the correct library length is still retrieved, despite the low electron dose. Atom-counts are shown in figure 6d. The atom-counts obtained from the analysis of this low dose image of the Pt/Ir nanoparticle differ no more than ± 1 atom as compared to the results obtained from the original, relatively low dose image of the Pt/Ir nanoparticle, as shown by the difference map in figure 6e.

We conclude from the results in the present section that the hybrid method for atom-counting holds promise for quantitative analysis of challenging, beam-sensitive nanoparticles, thanks to its ability to overcome challenges presented by very low electron doses.

6. Discussion and conclusions

In the present paper, an improved method for atom-counting from ADF STEM images of monotype crystalline nanostructures has been presented. This method was shown to exceed the limitations of the atom-counting methods that exist today, by directly combining image simulations and statistical parameter estimation theory. The method exploits prior knowledge obtained from image simulations, without suffering from the unknown accuracy of the experimental parameters used in these image simulations. It was shown that the largest progress is made for low dose images of small nanoparticles, conditions for which the statistics-based method can no longer obtain reliable atom-counts. This result is confirmed by the analysis of a small platinum-iridium nanoparticle imaged using a relatively low electron dose, which could not be analysed reliably using the statistics-based method, and by the successful analysis of a simulated low dose image.

It should be noted that the description of the performance for atom-counting in section 4 in fact assumes that the linear scaling relationship between simulated scattering cross sections and experimental scattering cross sections accurately describes the combined effect of measurement errors in different experimental input parameters of the image simulations. However, not all parameters used to perform the image simulations affect the scattering cross sections in a linear manner. Although it is shown that this linear scaling relationship provides a good first approximation, the performance of the hybrid method may improve by refining this parametric function. The hybrid method has nonetheless been shown to be a promising first step towards reliable atom-counting from low electron dose images of beam-sensitive materials.

Acknowledgments

The authors acknowledge financial support from the Research Foundation Flanders (FWO, Belgium) through project fundings (G.0374.13N, G.0368.15N, and G.0369.15N), and a postdoctoral research Grant to A. De Backer. The research leading to these results has received funding from the European Union Seventh Framework Programme under Grant Agreement 312483 - ESTEEM2 (Integrated Infrastructure Initiative-I3). The authors are grateful to G.T. Martinez for providing image simulations.

Appendix A. Model-based parameter estimation

An incoherent parametric imaging model to describe the expectation values of the image intensities of an ADF STEM image of crystalline nanomaterials is formulated by a function that is sharply peaked at the positions of the atomic columns, modelled as a superposition of Gaussian peaks. The expectation value of the image intensity at pixel (k, l) in the image is therefore given by:

$$O(\mathbf{r}_{k,l};\theta) = \zeta + \sum_{n=1}^{N} \eta_n \exp\left(-\frac{(x_k - \beta_{x_n})^2 + (y_l - \beta_{y_n})^2}{2\rho^2}\right). \tag{A.1}$$

In this expression, ζ is a constant background present in the image, ρ is the width of the two-dimensional Gaussian peaks, η_n is the height of the n^{th} Gaussian peak, β_{x_n} and β_{y_n} are the x- and y-coordinate of the n^{th} atomic column, and N is the total number of atomic columns in the image. The unknown parameters are summarised in the parameter vector:

$$\theta = (\beta_{x_1}, ..., \beta_{x_N}, \beta_{y_1}, ..., \beta_{y_N}, \rho, \eta_1, ..., \eta_N, \zeta)^T. \tag{A.2}$$

The intensities belonging to the different atomic columns can be quantified in two ways. Either the maximum value of the Gaussian peak is used, or the volume under the peak, which equals the total intensity of the scattered electrons. The volume under an estimated Gaussian peak expresses the so-called scattering cross section:

$$\hat{V}_n = 2\pi\hat{\eta}_n\hat{\rho}^2, \tag{A.3}$$

with $\hat{\eta}_n$ and $\hat{\rho}$ the least squares estimates for the parameters η_n and ρ from equation (A.1). The scattering cross sections have been shown to outperform the peak intensities for atom-counting [38].

Appendix B. Cramér-Rao lower bound

For unbiased estimators, the Cramér-Rao lower bound defines the lower bound on the variance [36, 37]:

$$\text{cov}(\mathbf{\Psi}_G) \geq F_{\mathbf{\Psi}_G}^{-1}, \tag{B.1}$$

with $\mathbf{\Psi}_G$ the vector containing the estimators, and $F_{\mathbf{\Psi}_G}$ the Fisher information matrix, which is defined as follows:

$$F_{\mathbf{\Psi}_G} = -\mathbb{E}\left[\left.\frac{\partial^2 \ln p(\mathbf{V};\mathbf{\Psi}_G)}{\partial\mathbf{\Psi}_G\partial\mathbf{\Psi}_G^T}\right|_{\mathbf{\Psi}_G=\mathbf{\Psi}_0}\right], \tag{B.2}$$

where $\mathbb{E}$ expresses the expectation value. In this expression, $p(\mathbf{V};\mathbf{\Psi}_G)$ represents the joint probability density

function, in this case determined by the Gaussian mixture model $f_{\mathrm{mix}}(\mathbf{V};\mathbf{\Psi}_G)$, which describes the probability distribution of the set of scattering cross sections $\mathbf{V}$, and is determined by the unknown parameters expressed by the parameter vector $\mathbf{\Psi_G}$. The vector $\mathbf{\Psi}_0$ contains the actual values of the parameters to be estimated. In practice, the following integral is numerically integrated:

$$F_{\mathbf{\Psi}_G} = -N \int_{-\infty}^{\infty} \frac{\partial^2 \ln f_{\mathrm{mix}}(V;\mathbf{\Psi}_G)}{\partial \mathbf{\Psi}_G \partial \mathbf{\Psi}_G^T}\bigg|_{\mathbf{\Psi}_G=\mathbf{\Psi}_0} f_{\mathrm{mix}}(V;\mathbf{\Psi}_G) dV, \quad \text{(B.3)}$$

with N the total number of columns in the image.

References

[1] T. J. Park, G. C. Papaefthymiou, A. J. Viescas, A. R. Moodenbaugh, S. S. Wong, Size-Dependent Magnetic Properties of Single-Crystalline Multiferroic $BiFeO_3$ Nanoparticles, Nano Letters 7 (2007) 766–772.

[2] H. J. Chen, X. S. Kou, Z. Yang, W. H. Ni, J. F. Wang, Shape- and Size-Dependent Refractive Index Sensitivity of Gold Nanoparticles, Langmuir 24 (2008) 5233–5237.

[3] J. N. Anker, W. P. Hall, O. Lyandres, N. C. Shah, J. Zhao, R. P. Van Duyne, Biosensing with plasmonic nanosensors, Nature Materials 7 (2008) 442–453.

[4] A. V. Crewe, J. Wall, L. M. Welter, A High-Resolution Scanning Transmission Electron Microscope, Journal of Applied Physics 39 (1968) 5861–5868.

[5] P. D. Nellist, S. J. Pennycook, The Principles and Interpretation of Annular Dark-Field Z-Contrast Imaging, Advances in imaging and electron physics 113 (2000) 147.

[6] S. J. Pennycook, L. A. Boatner, Chemically sensitive structure-imaging with a scanning transmission electron microscope, Nature 336 (1988) 565–567.

[7] J. M. Cowley, M. S. Hansen, S. Y. Wang, Imaging modes with an annular detector in STEM, Ultramicroscopy 58 (1995) 18–24.

[8] P. Hartel, D. Rose, C. Dinges, Conditions and reasons for incoherent imaging in STEM, Ultramicroscopy 63 (1996) 63–114.

[9] S. C. Anderson, C. R. Birkeland, G. R. Anstis, D. J. H. Cockayne, An approach to quantitative compositional profiling at near-atomic resolution using high-angle annular dark field imaging, Ultramicroscopy 69 (1997) 83–103.

[10] S. Van Aert, J. Verbeeck, R. Erni, S. Bals, M. Luysberg, D. Van Dyck, G. Van Tendeloo, Quantitative atomic resolution mapping using high-angle annular dark field scanning transmission electron microscopy, Ultramicroscopy 109 (2009) 12361244.

[11] G. T. Martinez, A. Rosenauer, A. De Backer, J. Verbeeck, S. Van Aert, Quantitative composition determination at the atomic level using model-based high-angle annular dark field scanning transmission electron microscopy, Ultramicroscopy 137 (2014) 12–19.

[12] J. M. LeBeau, S. D. Findlay, L. J. Allen, S. Stemmer, Standardless atom counting in scanning transmission electron microscopy, Nano Letters 10 (2010) 4405–4408.

[13] S. Van Aert, K. J. Batenburg, M. D. Rossell, R. Erni, G. Van Tendeloo, Three-dimensional atomic imaging of crystalline nanoparticles, Nature 470 (2011) 374–377.

[14] S. Bals, M. Casavola, M. A. van Huis, S. Van Aert, K. J. Batenburg, G. Van Tendeloo, D. Vanmaekelbergh, Three-Dimensional Atomic Imaging of Colloidal CoreShell Nanocrystals, Nano Letters 11 (2011) 3420–3424.

[15] S. Bals, S. Van Aert, C. P. Romero, K. Lauwaet, M. J. Van Bael, B. Schoeters, B. Partoens, E. Yücelen, P. Lievens, G. Van Tendeloo, Atomic scale dynamics of ultrasmall germanium clusters, Nature Communications 3 (2012) 897.

[16] L. Jones, K. E. MacArthur, V. T. Fauske, A. T. J. van Helvoort, P. D. Nellist, Rapid estimation of catalyst nanoparticle morphology and atomic-coordination by high-resolution Z-contrast electron microscopy, Nano Letters 14 (2014) 6336–6341.

[17] J. J. Geuchies, C. van Overbeek, G. B. Evers, W. H. and, A. De Backer, G. P. Gantapara, F. T. Rabouw, J. Hilhorst, J. L. Peters, O. Konovalov, A. V. Petukhov, M. Dijkstra, L. D. A. Siebbeles, S. Van Aert, S. Bals, D. Vanmaekelbergh, In situ study of the formation mechanism of two-dimensional superlattices from PbSe nanocrystals, Nature Materials 15 (2016) 1248–1254.

[18] F. Moyon, D. Hernandez-Maldonado, M. D. Robertson, A. Etienne, C. Castro, W. Lefebvre, Reverse Monte Carlo reconstruction algorithm for discrete electron tomography based on HAADF-STEM

atom counting, Journal of Microscopy 265 (2017) 73–80.

[19] A. De Backer, G. T. Martinez, A. Rosenauer, S. Van Aert, Atom counting in HAADF STEM using a statistical model-based approach: Methodology, possibilities, and inherent limitations, Ultramicroscopy 134 (2013) 23–33.

[20] S. Van Aert, A. De Backer, G. T. Martinez, B. Goris, S. Bals, G. Van Tendeloo, Procedure to count atoms with trustworthy single-atom sensitivity, Physical Review B 87 (2013) 064107.

[21] H. E, K. E. MacArthur, T. J. Pennycook, E. Okunishi, A. J. D'Alfonso, N. R. Lugg, L. J. Allen, P. D. Nellist, Probe integrated scattering cross sections in the analysis of atomic resolution HAADF STEM images, Ultramicroscopy 133 (2013) 109119.

[22] A. Rosenauer, T. Mehrtens, K. Müller, K. Gries, M. Schowalter, P. V. Satyam, S. Bley, C. Tessarek, D. Hommel, K. Sebald, M. Seyfried, J. Gutowski, A. Avramescu, K. Engl, S. Lutgen, Composition mapping in InGaN by scanning transmission electron microscopy, Ultramicroscopy 111 (2011) 1316–1327.

[23] A. De Backer, K. H. W. van den Bos, W. Van den Broek, J. Sijbers, S. Van Aert, StatSTEM: An efficient approach for accurate and precise model-based quantification of atomic resolution electron microscopy images, Ultramicroscopy 171 (2016) 104–116.

[24] L. Jones, Quantitative ADF STEM: acquisition, analysis and interpretation, IOP Conf. Series: Materials Science and Engineering 109 (2016) 012008.

[25] C. Dwyer, C. Maunders, C. L. Zheng, M. Weyland, P. C. Tiemeijer, J. Etheridge, Sub-0.1 nm-resolution quantitative scanning transmission electron microscopy without adjustable parameters, Applied Physics Letters 100 (2012) 191915.

[26] S. D. Findlay, J. M. LeBeau, Detector non-uniformity in scanning transmission electron microscopy, Ultramicroscopy 124 (2013) 52–60.

[27] T. Mehrtens, M. Schowalter, D. Tytko, P. Choi, D. Raabe, Measurement of the indium concentration in high indium content InGaN layers by scanning transmission electron microscopy and atom probe tomography, Applied Physics Letters 102 (2013) 132112.

[28] G. T. Martinez, L. Jones, A. De Backer, A. Béché, J. Verbeeck, S. Van Aert, P. D. Nellist, Quantitative STEM normalisation: The importance of the electron flux, Ultramicroscopy 159 (2015) 46–58.

[29] F. F. Krause, M. Schowalter, T. Grieb, K. Müller-Caspary, T. Mehrtens, A. Rosenauer, Effects of instrument imperfections on quantitative scanning transmission electron microscopy, Ultramicroscopy 161 (2016) 146–160.

[30] A. J. den Dekker, S. Van Aert, A. van den Bos, D. Van Dyck, Maximum likelihood estimation of structure parameters from high resolution electron microscopy images. Part I: a theoretical framework, Ultramicroscopy 104 (2005) 83106.

[31] A. J. den Dekker, J. Gonnissen, A. De Backer, J. Sijbers, S. Van Aert, Estimation of unknown structure parameters from high-resolution (S)TEM images: What are the limits?, Ultramicroscopy 134 (2013) 34–43.

[32] G. McLachlan, D. Peel, Finite Mixture Models, Wiley series in probability and statistics. John Wiley and Sons, inc., 2000.

[33] A. De Backer, G. T. Martinez, K. E. MacArthur, L. Jones, A. Béché, P. D. Nellist, S. Van Aert, Dose limited reliability of quantitative annular dark field scanning transmission electron microscopy for nanoparticle atom-counting, Ultramicroscopy 151 (2015) 56–61.

[34] J. C. Meyer, J. Kotakoski, C. Mangler, Atomic structure from large-area, low-dose exposures of materials: A new route to circumvent radiation damage, Ultramicroscopy 145 (2014) 13–21.

[35] J. M. LeBeau, S. D. Findlay, L. J. Allen, S. Stemmer, Quantitative Atomic Resolution Scanning Transmission Electron Microscopy, Physical Review Letters 100 (2008) 206101.

[36] C. R. Rao, Information and the Accuracy Attainable in the Estimation of Statistical Parameters, Bulletin of the Calcutta Mathematical Society 37 (1945) 81–89.

[37] H. Cramér, Mathematical Methods of Statistics, New York: Princeton University Press, 1946.

[38] A. De Backer, A. De wael, J. Gonnissen, S. Van Aert, Optimal experimental design for nanoparticle atom-counting from high-resolution STEM images, Ultramicroscopy 151 (2015) 46–55.